Automated 3D Segmentation and Analysis of Cotton Plants

Anthony Paproki, Jurgen Fripp, Olivier Salvado
CSIRO ICT,
The Australian e-Health Research Centre
Brisbane, Australia
Anthony.Paproki@csiro.au

Xavier Sirault, Scott Berry, Robert Furbank
CSIRO Plant Industry,
The High Resolution Plant Phenomics Centre
Canberra, Australia

Abstract— **One of the main challenges in high-throughput plant data acquisition is the robust and automated analysis of the data. This includes a high-resolution 3D plant model reconstruction and an automated 3D segmentation. In this paper we present our top-down partitioning pipeline used to automatically segment high-resolution plant meshes. The proposed method produces a smart partition of the initial mesh that allows to identify the main stem, branches, and leaves of the plant. Extracted regions are then processed through the next stage of the automated analysis, which retrieves accurate plant information such as stem length, leaf width, length or area. Results involved applying our top-down approach on a prototype population of 6 cotton-plant meshes studied at 3 or 4 time points. Using our partitioning pipeline, we obtained accurate meshes segmentations for 20 plants out of the initial 22. Results validate the feasibility of an automated analysis of plant data. Future work will involve extending our approach to multiple plant varieties and using an atlas-based iterative feedback scheme to improve the 3D plant reconstruction.**

I. INTRODUCTION

Plant phenomics research delves into *deep plant phenotyping* and *reverse phenomics*, fields of study focusing on the metabolism and physiological processes of plants, and analysing new plant's traits to understand their mechanistic basis. The current aim of the plant phenomics research is to build realistic plant modelling systems. To this end, the "High-Resolution Plant Phenomics Centre", associated with "Neo Vista System Integrators" has built an advanced platform for high-throughput non-invasive plant phenomics data acquisition: *PlantScan*. This automated plant scanning platform captures high-resolution stereographic, multi-spectral and infrared images, and Light Detection and Ranging Sensors data. These data cubes are used to produce a full 3D surface mesh reconstruction of each plant with overlaid spectral information. As noted in a recent study [1], performing plant phenotyping requires high-throughput plant data acquisition of several thousands plants per day. *PlantScan* has been designed to acquire and analyse 3000 plants per day (≈ 2 Terabytes of data per day). Manual measurements for all the data is impractical, hence, the development of automated solutions is essential. This involves developing a fully automated software solution providing advanced features such as plant limbs recognition (stem, branches, leaves, etc.), accurate data extraction (stem size, leaf width, length, and area), longitudinal measurements and plant-part tracking over time.

The pilot study developed in this paper involved processing prototype plant surface meshes previously reconstructed using the manually acquired images of 6 plants studied over 4 time-points and using 3DSOM [9], a software for 3D scanning. We investigate the feasibility of developing an automatic and robust image and mesh based segmentation pipeline to process the large amount of data that will be acquired using the *PlantScan*. We particularly focus on the robust and accurate extraction of morphological features from the surface meshes.

A recent survey on mesh segmentation techniques [2] classified the segmentation algorithms into 2 categories: *part-type* and *surface-type* segmentation algorithms. For the semantic features extraction, we are interested in the *part-type* segmentation, which aims at extracting physical meaningful parts from the initial mesh. In the literature, numerous 3D-model segmentation techniques are available [2,3]. This includes region-growing algorithms [2,11], convenient since the criteria used to constrain the growth of a region is flexible, primitives-fitting algorithms [4,12], applicable to plant segmentation considering that similar basic shapes are found on different parts of the plants (branches, leaves), and symmetry based segmentations [14], useful when the mesh to segment contains symmetries. In addition, top-down segmentation designs [18], that gradually and recursively partition a mesh into more precise regions, have proved to be robust to mesh deformations and noise, which is a non-negligible advantage in the case of reconstructed plant meshes segmentation. Since cotton plants are variable in shapes, no algorithm, singly applied, is robust enough to provide an accurate segmentation in all cases. Unlike applied domains such as human body morphological segmentation [5] or medical imaging [15,16,17], that use advanced approaches for mesh segmentation, the applied domain of plant meshes partitioning lacks background material, the few existing papers describing semi-automatic [6] or 2D segmentation methods [7].

Therefore, as an addition to the plant mesh segmentation domain, we propose a hybrid top-down approach that combines the different generic algorithms presented before in a step-wise automated segmentation pipeline that refines the segmentation at each completed step. Each stage of the pipeline aims at extracting a given limb from the plant mesh or at extracting a targeted sub-mesh that will be used as input at another step of the algorithm. Our design relies on the regularity of the cotton plant architecture that allows an iterative application of a given algorithm on similar parts of the plant.

978-0-7695-4588-2/11 $26.00 © 2011 IEEE
DOI 10.1109/DICTA.2011.99

The remainder of the paper is organized as follow. In section II, we give a full explanation of the pipeline we built to qualitatively and quantitatively study the plants. The performances of our design are described in section III, and finally, we sum-up this paper by sharing our conclusions on an automated analysis of the plant phenomics and introducing the future work planed in this field of research.

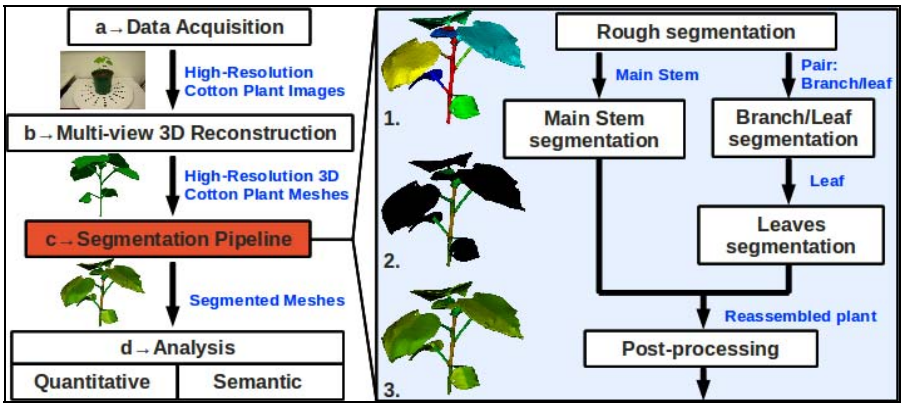

Figure 1. Analysis pipeline. a, b, c, d are the main steps of the pipeline and 1, 2, 3 illustrations of the segmentation steps.

II. METHODOLOGY

The acquisition and processing pipeline is illustrated in Fig. 1 and consists of 4 main stages: a plant data acquisition, a multi-view 3D reconstruction, presented in sections *II.B* and *II.C*, an automated 3D segmentation of plant models, and an automated analysis of the segmented plant meshes, respectively presented in sections *II.D* and *II.E*.

A. Prototype population

Twenty-two plant meshes were used to evaluate our segmentation pipeline: 6 different plants studied at 4 time-points, except for two plants that were studied only for 3 time-points (due to data acquisition issues). For each plant and each time-point, scientists from HRPPC performed manual measurements of plant data such as stem length, leaves width and length. The manual measurements were used as ground truth in order to validate the accuracy of the segmentation and data extraction.

B. Plant data Acquisition

Images were captured using a high-resolution Pentax K10 camera with a sigma 20-40mm aspherical lens. Each cotton plant pot was placed at the centre of a rotating tray over a 3DSOM calibration pattern (see section *II.C*). The camera was fixed on a tripod during all the acquisition process. The Lazy Susan was manually rotated and pictures were taken at each rotation angle. The acquisition process finished, 64 images were available (for each plant and at each time-point) for the multi-view 3D reconstruction (see section *II.C*). The image resolution was 3872x2592 (~10 million) pixels. An example of an acquired plant image is shown on Fig. 1. *PlantScan* will make this laborious acquisition process fully automatic.

C. Multi-view based 3D reconstruction

This stage involved reconstructing high-resolution meshes of plants using the previously acquired high-resolution images (see *II.B*). Scientists from HRPPC performed the 3D reconstruction. For this prototype population, they used 32 out of the 64 images, acquired per plant and date, as inputs to the reconstruction pipeline of 3DSOM [9], a 3D scanning system.

The reconstruction pipeline of 3DSOM includes a pre-processing step that extracts the object of interest from the input images and calibrates the camera using a known pattern present in the image. Then, a "direct-intersection shape from silhouette" approach extracts the visual hull (maximum volume containing the object) from the images. A wiring-up algorithm is used to build the final reconstructed mesh using the visual hull vertices [9]. The resolution of the reconstructed meshes fluctuates between 120000 and 270000 polygons. This step of the pipeline will be fully automated using a customized 3D reconstruction algorithm such as the "Embedded Voxel Colouring" algorithm [10].

D. Plant meshes segmentation pipeline

The 3D segmentation pipeline partitions the plant meshes into different meaningful parts: main stem, branches, and leaves. We segment a mesh by assigning a unique integer value (called label) to all the vertices of a same partition. The pipeline is subdivided into different steps, each consisting of a generic algorithm and acting at a different precision level.

- The first pass, derived from [2,11], is based on a *mesh-attributes* constrained *region-growing* design. It takes as input the non-partitioned plant mesh and segments it into coarse regions: the stem and *n* regions for the pairs of branches and leaves (see *II.D.1*).
- Inspired by [4,12,13], a second pass uses the regions obtained in the first pass as inputs for the next steps of the method, consisting of 2 "*tubular-shape-fitting"* based segmentations designed to partition the stem into relevant parts and detach the branches from the leaves (see section *II.D.2* and *II.D.3*).
- Isolated leaves are then processed by a *symmetry-based* method [14] that finds the best cut-plane that splits a leaf into two parts. This is the deepest level of segmentation of our top-down approach (see *II.D.4*).

- Finally, a post-processing step including an *adaptive region-growing* [2,11] algorithm is used to sharpen the segmentation (see *II.D.5*).

A detailed description of each stage is provided in the next paragraphs. For the rest of the paper, we consider that we are working in a direct, z-up, and Euclidean coordinates system, and that $\omega = \{p_1, p_2, ..., p_m\}$ represents the set of vertices of the mesh to segment (m being the total number of vertices). We also denote $d(p_1, p_2)$ and $D(p_1, p_2)$ respectively the planar Euclidean distance (on plane (x,y)) and the 3D Euclidean distance between p_1 and p_2.

1) Step 1: Region-Growing based rough segmentation

The aim of the first pass is to roughly segment the plant meshes. For a given plant holding n leaves, this involves segmenting the mesh into $n+1$ regions: *1* for the main stem, and n for the pairs of branches and leaves.

Let c denote the plant centre; we retrieve c by finding the lowest vertex of the mesh, which represents the bottom of the main stem. Let r_1 and r_2 denote radii from c such that r_1 is the inner radius within which a vertex p_i is always part of the main stem region and r_2 the outer radius after which a vertex is not part of the main stem region. The range of vertices belonging to $[r_1; r_2]$ remains undetermined. To classify them, we retrieve the normal $\vec{n}$ for each vertex and compute the angle α between n and the *z-axis*. A vertex p_i is considered part of the stem region if α belongs to a predefined range. Mathematically, having R_1 and R_2 sets of vertices verifying (1) and (2), the set of vertices *"S"* defining the stem is formulated by (3):

$$R_1 = \{p_i \in \omega \mid d(p_i, c) \le r_1\} \quad (1)$$

$$R_2 = \{p_i \in \omega \mid r_1 \le d(p_i, c) \le r_2, \left(\frac{\Pi}{3} \le \alpha \le \frac{2\Pi}{3}\right)\} \quad (2)$$

$$S = R_1 \cup R_2 \quad (3)$$

Once the stem partition is defined, we use a region-growing algorithm to create the other regions. We start from a point that is not in the stem region, the seed, and grow a new label to all the eligible topological neighbours. A neighbour is eligible if it does not belong to any region yet. The algorithm terminates when there are no neighbours remaining i.e. all neighbours are already marked with a region label. We go through all the vertices of the plant and grow a new region each time we find a non-labelled vertex (not part of any region → a new seed). A typical result of this pass is presented on Fig. 1.1.

2) Step 2: Shape fitting based stem segmentation

Shape fitting segmentation algorithms consist of finding a given shape (known a priori) in a complex mesh and to consider that all the vertices within the matched shape belong to the same region. This part of the pipeline uses as input the previously extracted stem. Assessing that the cotton plant main stem follows a tubular shape, we build the closest matching tube around the stem so as to narrow the previous coarse segmentation.

To create the tube shape, we create a curve that follows the stem and build the tube around it. Let's define h as the highest point of the stem region. We start by creating a straight line, constituted of n regularly spaced points ($l_1, l_2, ..., l_n$) and going from c to h. We then go through the points of the line, $l_2, ..., l_{n-1}$, and interpolate their accurate position along the stem using the vertices p_j belonging to their neighbourhood V_i defined by (4). The new coordinates of a given li are equal to the average coordinates of its neighbourhood's vertices.

$$V_i(l_i) = \{p_j \in S \mid \Delta z(p_j, l_i) \le C_1, d(p_j, l_i) \le C_2\} \quad (4)$$

with C_1 et C_2 defined constants, Δz the absolute height difference and d the planar distance.

The tube is then created around the curve using a parameterized radius R. From then, each vertex inside the tube is definitively considered as part of the main stem region. We create a new region U (Uncategorized) for the vertices that previously belonged to the coarse stem region and that are not in the tube. This region is made of vertices that should belong to branch regions. Fig. 2a/b illustrate the curve and tube fitting along the stem.

Once we have a sharply defined stem, we can segment it into relevant parts. A stem part, defined by $Part_i$, begins at a junction J_i between a branch B_i and the stem and goes up to the next junction J_{i+1}. We use the vertices from U to define the junctions. Mathematically, the set of vertices p_k belonging to $Part_i$ is defined by (5). Fig. 2c shows the sharply segmented main stem obtained after this pass.

$$Part_i(J_i, J_{(i+1)}) = \{p_k \in S \mid J_{iz} \le p_{kz} < J_{(i+1)z}\} \quad (5)$$

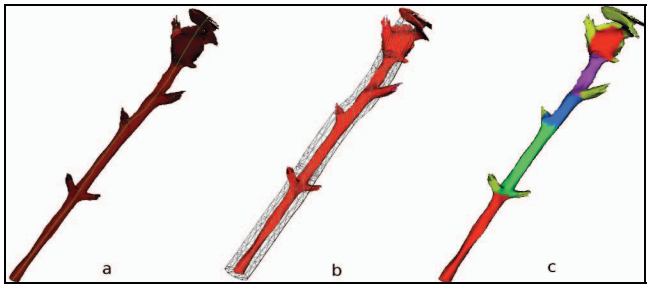

Figure 2. Visualization of: a) the curve following the stem, b) the tube shape used to segment the stem and c) the segmented stem.

3) Step3: Shape fitting based branch segmentation

This step uses the previously segmented pairs of branches and leaves as inputs. In a process similar to the one leading to the creation of the tubular shape following the stem, we implemented a shape-fitting algorithm that, for a given pair branch/leaf, splits the pair into two different regions: a branch and a leaf.

In this case, the curve starts from the point closest to main stem and goes to the tip of the leaf (maximum planar distance

from *c,* see P_{max} on Fig. 3c). To interpolate the position of a given point *li* of the curve along the branch or the leaf, we first adjust its height to the interpolated height of the previous point, and then, find its neighbourhood V_i, defined by (6), using a standard 3D Euclidian distance *D*. Again, the position of l_i is the average of the positions of the vertices of the neighbourhood *Vi*.

$$V_i(l_i) = \{p_j \in \Gamma_k \mid D(p_j, l_i) \leq C\} \quad (6)$$

with Γ_k set of vertices belonging the pair *k* (branch *k* + leaf *k*) and C a predefined constant distance.

We create the tube shape similarly as in section *II.D.2* (see Fig. 3a), and use it to separate the branch from the leaf. Let I_k and O_k, denote respectively the set of vertices inside and outside the tube. Let's then define p_{min} as the vertex from O_k which is the closest to *c* in terms of planar distance *d* (see Fig. 3c) then, the sets of vertices defining the branch B_k and the leaf L_k are given by (7) and (8). Fig. 3b shows a result obtained on a pair branch/leaf. Fig 1.2 illustrates the mesh segmentation after this pass.

$$B_k = \{p_j \in \Gamma_k \mid d(p_j, c) \leq d(p_{\min}, c)\} \quad (7)$$

$$L_k = \{p_j \in \Gamma_k \mid pj \notin B_k\} \quad (8)$$

4) Step 4: Symmetry based leaf segmentation

The leaf segmentation algorithm has to be robust to the numerous natural leaf shape variations (folded leaves, leaf shape changing over time) and poor leaf reconstructions due to occlusions during the reconstruction process (leaf thickness, leaves stuck together). The more effective solutions are based on a property that is common to the majority of the leaves: the symmetry. We investigated multiple approaches such as symmetry plane parameters optimization [11], but the more satisfying leaf segmentations were obtained by a 2D symmetry.

The same algorithm is applied to each separate leaf. Let p_{max} be the point that is the further from the plant centre *c*. And let p_1 be a point of the leaf. If we consider the 2D vectors (on plane (x,y)) from *c* to p_{max} and from *c* to p_1, the region in which p_1 belongs to is given by the sign of the angle α between the two vectors (see Fig. 3c). Let S_{1k} and S_{2k} be the sets of vertices belonging to each side of the leaf *k*. We mathematically define S_{1k} and S_{2k} by (9).

$$S_{1k} = \{p_j \in L_k \mid \alpha \leq 0\} \text{ and } S_{2k} = \{p_j \in L_k \mid \alpha > 0\} \quad (9)$$

A basic segmentation evaluation involves using the current regions of the leaf in order to compute the symmetry plane π of the leaf. Using vertices from S_{1k} and S_{2k} and the plane π, we retrieve the 2 maximum projection distances on each side of π (d_{S1k} and d_{S2k}) and consider the segmentation satisfactory if ρ verifies (10). If (10) is not verified, we repeat the segmentation process using the centre of the leaf c_{leaf} instead of p_{max}. We then keep the solution that minimizes the absolute difference between d_{S1k} and d_{S2k}.

$$\rho \leq K \text{ with } \rho = \frac{\max(d_{S_{1k}}, d_{S_{2k}})}{\min(d_{S_{1k}}, d_{S_{2k}})} \text{ and } K \text{ a given distance} \quad (10)$$

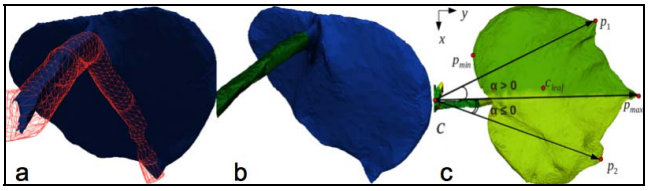

Figure 3. a) The tube shape used to extract the branch, b) the separated branch and leaf, c) a schematic explanation of the leaf segmentation.

5) Step 5: Post-processing step

The post-processing step sharpens the segmentation and removes all the leaks that might have escaped the segmentation process. For instance, as a first pass, we assign to the proper regions the vertices belonging to *U* (see *II.D.2* and yellow region on Fig. 2c). The shared property of those vertices is that they belong to a branch; hence, they have to be added to the appropriate branch region.

To perform this first pass, we use an adaptive region-growing algorithm. The seeds for the region growing are the vertices from *U* that share an edge with a vertex from a branch region B_k (see *II.D.3*). Starting from the seeds, we recursively and gradually grow the considered branches labels to all the topological neighbours that belong to the region *U*.

A second simple post-processing pass involves assigning isolated vertices to a region from their neighbourhood. A vertex is considered isolated when none of its topological neighbours belongs to the same region as the studied vertex.

E. Computation of plant information

In this section, we detail how, using the segmented meshes, we computed plant information such as stem length, leaf width and leaf length. We also explain how we managed to quantify the error on the measurements by comparing them with the ground truth.

For the next paragraphs, Ω stands for the number of plants (here 6), Φ stands for the number of time-points (3 or 4), and a_{ij} and m_{ij} respectively denote the automated and manual measurements of the stem length for the plant *i* at time-point T_j, with $1 \leq i \leq \Omega$ and $0 \leq j < \Phi\text{-}1$.

1) Main stem length

To compute the main stem length, we locate the highest and lowest vertices in the stem regions and compute their absolute height difference. Since initial study cases haven't been subject to a precise camera calibration, to be able to compare the automated measurements with ground truth, we first need to define a conversion ratio from the mesh unit to the manual-measurement unit (mm). We compute this scaling ratio λ by applying (11).

$$\lambda = \frac{\sum_{i=1}^{i=\Omega}\left(\sum_{j=0}^{j=\Phi-1}\frac{a_{ij}}{m_{ij}}\right)}{\Omega+\Phi} \qquad (11)$$

Using λ, we scale the automatically retrieved data such that $g_{ij} = \lambda \times a_{ij}$, with g_{ij} scaled value of a_{ij}. With comparable data, we can compute an average error E between ground truth and experimental measurements using (12).

$$\mathrm{E} = \frac{\sum_{i=1}^{i=\Omega}\left(\sum_{j=0}^{j=\Phi-1}\varepsilon_{ij}\right)}{\Omega+\Phi} \quad \text{with} \quad \varepsilon_{ij} = \frac{|g_{ij}-m_{ij}|}{|g_{ij}+m_{ij}|} \qquad (12)$$

2) Leaves width and length

To compute a leaf width, we first locate the leaf, and, using the previously computed symmetry plane, we retrieve one point on each side of the leaf such that they maximize the sum of the projection distances to the cut plane. The maximized sum is the leaf width. For the leaf length, we only consider the vertices that belong, or are close enough to the cut plane and keep the two that are the further apart. The Euclidean distance between these two points is the leaf length.

Error measurements were also performed for the leaves width and length. The difference with the formulas used for the main stem is that we loop over the plants leaves. Let Ψ_{ij} denote the number of leaves of the plant i at time-point T_j (Ψ being the total number of leaves) and a_{ijk}(resp. m_{ijk}) denote the automated (resp. manual) measurements (width or length) of the leaf k for the plant i at time T_j. Adapted formulas are given in (13) (14).

$$\lambda = \frac{\sum_{i=1}^{i=\Omega}\left(\sum_{j=0}^{j=\Phi-1}\left(\sum_{k=1}^{k=\Psi_{ij}}\frac{a_{ijk}}{m_{ijk}}\right)\right)}{\Omega+\Phi+\Psi} \;;\; g_{ijk} = \lambda \times a_{ijk} \qquad (13)$$

$$\mathrm{E} = \frac{\sum_{i=1}^{i=\Omega}\left(\sum_{j=0}^{j=\Phi-1}\left(\sum_{k=1}^{k=\Psi_{ij}}\varepsilon_{ijk}\right)\right)}{\Omega+\Phi+\Psi} \text{ with } \varepsilon_{ijk} = \frac{|g_{ijk}-m_{ijk}|}{|g_{ijk}+m_{ijk}|} \qquad (14)$$

III. Experimental Results

In this section, we present the results we obtained by applying our segmentation method on the prototype dataset of meshes (see *II.A*). As explained before, we used the manual measurements performed on each plant as ground truth.

As illustrated by the typical results of Fig. 5, our algorithm performed well, i.e. stem, branches and leaves are sharply identifiable, and is robust to the major reconstruction issues (see Fig. 4a/b). Moreover, the longitudinal analysis presented on Fig. 6 shows that, using our automated analysis we obtained quantitative results similar to ground truth in most cases for the stem length and leaves width. By applying (12)(14), we obtained the negligible average errors $\mathbf{E_s \approx 4.0\%}$ (≈ 6.4 mm on an average stem size of 161mm) and $\mathbf{E_w \approx 3.8\%}$ (≈ 3.1 mm on an average leaf width of 84.2mm) on the main stem size and leaves width measurements, and the non-negligible average error $\mathbf{E_l \approx 9.7\%}$ (≈ 6.58 mm on an average leaf length of 67.3mm) on the leaves length measurements.

The main weakness of our algorithm is illustrated on Fig 4c. Occlusions during the 3D reconstruction sometimes cause the apparition of a bundle at the top of the stem that can't be segmented using standard segmentation algorithms. The use of *PlantScan* images and a custom reconstruction algorithm constrained by light detection and ranging sensors data will solve the major reconstruction problems illustrated on Fig. 4a/b/c, and since our results, qualitative as well as quantitative, mainly depend on the quality of the reconstruction, it will also lead to better plant meshes segmentations and a more accurate data extractions.

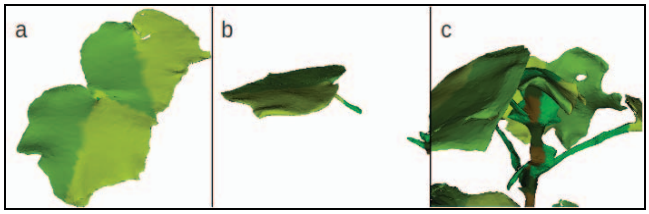

Figure 4. Robustness to a) leaves stuck together, b) holes in the mesh. The current main issue: c) top-bundle at the top of the main stem.

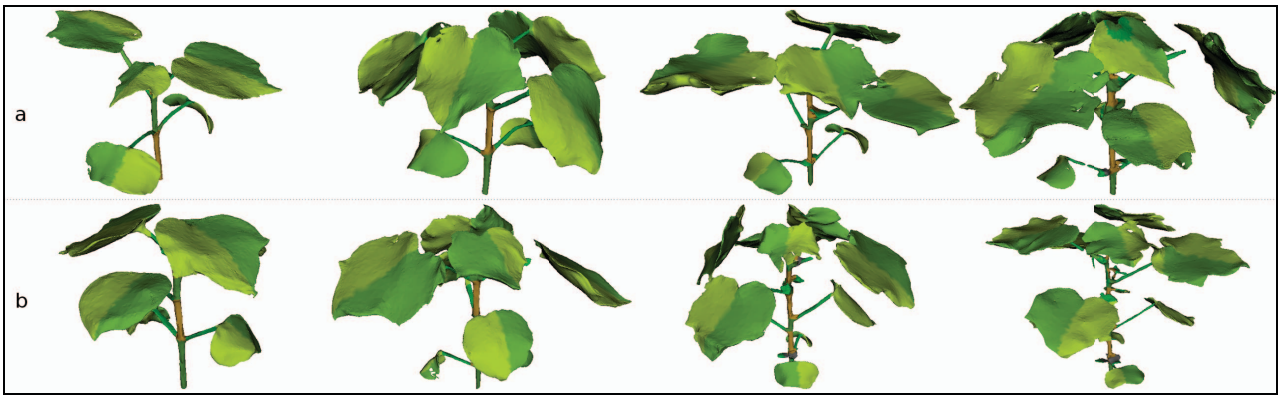

Figure 5. Qualitative segmentation results for 2 plants *a* and *b* over 4 time-points.

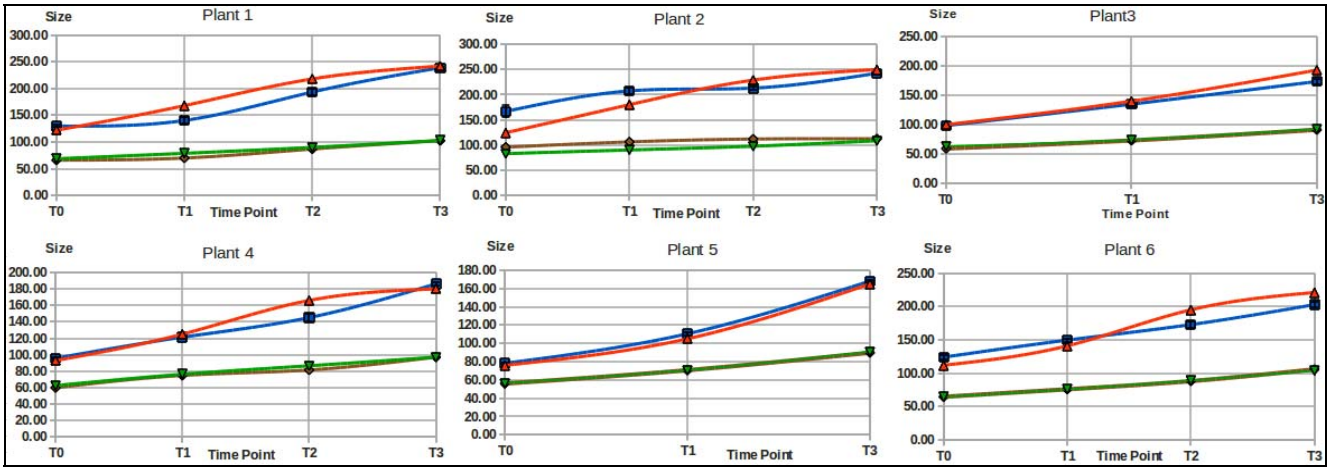

Figure 6. Longitudinal comparison of the automated measurements with ground truth. The graphs represent the stem size and average leaves width in millimetres over the 3 or 4 time-points. Red and blue → manual and automated stem length. Green and brown → manual and automated average leaves width.

CONCLUSION

In this paper, we presented a top-down 3D segmentation pipeline used to automatically partition an initial set of 22 cotton-plant meshes. Plant shape variations and reconstruction issues (leaves occlusions) make of the development of a robust segmentation algorithm a challenging task.

From the qualitative results presented in section III, we can conclude that our top-down approach is valid in the perspective of a morphological segmentation. Our pipeline allows the extraction of the meaningful limbs of the plant, which demonstrates certain robustness to the main shape variations and reconstruction issues. From a quantitative point of view, the tiny error percentages on the stem length and leaves width measurements validate the plausibility of an accurate automated analysis. However, the non-negligible error on the leaves length measurements, 9.7%, demonstrates that work has still to be done in order to obtain a complete and precise analysis.

Further work will involve using information from the segmented meshes and light detection and ranging sensors data in an iterative feedback scheme aiming at improving the 3D reconstructions of the plants. The improved 3D models will again be processed through the segmentation pipeline and more accurate data will be extracted. The process will be repeated until the extracted data are considered optimal.

REFERENCES

[1] M. Eberius, J. Lima-Guerra, "High-Throughput Plant Phenotyping – Data Acquisition, Transformation, and Analysis", in Bioinformatics, Tools and Applications, D. Edwards, J. Stajich, D. Hansen, Eds Springer, pp. 259–278, 2009.

[2] A. Shamir, "A survey on Mesh Segmentation Techniques", in Computer Graphics Forum, Vol. 27, 6th edition, pp. 1539–1556, September 2008.

[3] M. Attene, S. Katz, M. Mortara, G. Patane, M. Spagnuolo, A. Tal, "Mesh Segmentation - A Comparative Study", IEEE International Conference on Shape Modeling and Applications, 6th ed., 2006.

[4] M. Attene, B. Falcidieno, M. Spagnuolo, "Hierarchical segmentation based on fitting primitives", in The Visual Computer, Vol 22, Eds Springer, pp. 181–193, 2006.

[5] M. Mortara, G. Patane, M. Spagnuolo, "From geometric to semantic human body models", in Computers & Graphics, Vol. 27, pp. 1539–1556, 2008.

[6] L. Quan, P. Tan, G. Zeng, L. Yuan, J. Wang, S. B. Kang, "Image-based Plant Modeling" in ACM SIGGRAPH 2006 Papers, pp. 599–604, 2006.

[7] S. Gebhardt, W. Kuhbauch , "A new algorithm for automatic Rumex obtusifolius detection in digital images using colour and texture features and the influence of image resolution" in Precision Agriculture, Vol 8, Eds Springer, pp. 1–13, 2007.

[8] A. Golovinskiy, T. Funkhouser, "Consistent Segmentation of 3D models", in Computer & Graphics, vol. 33, Eds. Elsevier, 2009.

[9] A. Baumberg, A. Lyons, R. Taylor, "3D S.O.M.—A commercial software solution to 3D scanning", in Graphical Models 6th ed., vol. 67, pp. 476–495, November 2005.

[10] C. Sun, H. Talbot, S. Ourselin, T. Adriaansen, "Embedded Voxel Colouring" in Proceedings of the Seventh International Conference on Digital Image Computing: Techniques and Applications, DICTA 2003.

[11] M. Vieira, K. Shimada, "Surface mesh segmentation and smooth surface extraction through region growing" in Computer aided geometric design, Vol 22, Issue 8, 2005.

[12] M. Mortara, G. Patanè, M. Spagnuolo, B. Falcidieno, J. Rossignac, "Plumber: a method for a multi-scale decomposition of 3D shapes into tubular primitives and bodies" in Proceedings of the ninth ACM symposium on Solid modeling and applications, pp. 339–344, June 2004.

[13] J. Tierny, JP. Vandeborre, M. Daoudi , "Topology driven 3D mesh hierarchical segmentation" in Proceedings of the IEEE International Conference on Shape Modeling and Applications, pp. 215–220, 2007.

[14] J. Podolak, P. Shilane, A. Golovinskiy, S. Rusinkiewicz, T. Funkhouser, "A Planar-Reflective Symmetry Transform for 3D Shapes" in ACM Transactions on Graphics, Vol 25, pp. 549–559, 2006.

[15] J. Fripp, S. Crozier, S.K. Warfield, S. Ourselin, "Automatic segmentation of the knee bones using 3D active shape models", in International Symposium on Biomedical Imaging: From Nano to Macro, Washington, pp. 336–339 , April 2007.

[16] J. Fripp, P. Bourgeat, S. Crozier, S.n Ourselin, "Shape based segmentation of MRIs of the knee using phase and magnitude information", in Academic Radiology, Vol 14, 1201–1208, October 2007.

[17] T. Heimann, H.P. Meinzer, "Statistical shape models for 3D medical image segmentation: A review", in Medical Image Analysis, Vol 13, Issue 4, Pages 543-563, August 2009.

[18] F.D. Goes, S. Goldenstein, L. Velho, "A Hierarchical Segmentation of Articulated Bodies" in Computer Graphics Forum, Vol 27, Issue 5, pp. 1349–1356, July 2008.